Appl. Phys. B 46, 95–102 (1988)

Applied Physics B Photophysics and Laser Chemistry

Vibrational Relaxation of KrF* and XeCl* by Rare Gases

A. Kvaran

Science Institute, University of Iceland, JS-107 Reykjavik, Iceland

M. J. Shaw

Laser Division, Rutherford Appleton Laboratory, Didcot, OX11 OQX, U.K.

J. P. Simons

Chemistry Department, University of Nottingham, Nottingham, NG7 2RD, U.K.

Received 6 December 1987/Accepted 13 January 1988

Abstract. A steady-state, chemiluminescence technique has been used to measure effective rate constants for vibrational relaxation as a function of vibrational level for KrF* in collisions with He, Ne, and Ar and XeCl* with Ar. The effective rate constants reported include contributions to relaxation due to intersystem crossing between the B and C states, in addition to direct relaxation within the B state. The relevance of these results to the understanding of previous measurements in KrF and XeCl lasers is discussed.

PACS: 42.55 Hq, 78.60 Ps, 82.40 Tc

Recent demonstrations of the amplification of subpicosecond pulses to high-energy in KrF [1] and XeCl [2] lasers have refocused attention on the need to understand more fully the kinetic processes which determine the gain dynamics of the upper laser level. Of these, the most important are vibrational relaxation and mixing of the B ($\Omega=1/2$) and C ($\Omega=3/2$) states since they determine the effective pumping rate into the low-lying ($v'=0$–4) vibrational levels of the B state which contribute most strongly to the laser transition [3]. For short pulses, these processes determine the gain recovery time and can also modify the observed saturation energy of a laser amplifier. Vibrational relaxation is also important in long-pulse lasers where its competition with quenching affects the overall laser efficiency [4]. This is particularly relevant to KrF since this laser is a prime candidate for inertial confinement fusion and high laser efficiency is of paramount importance [5].

There have been a number of previous observations of the effects of vibrational relaxation in KrF lasers. By comparing either the suppression of fluorescence or saturation of gain during lasing with that predicted by simple models, a phenomenological relaxation rate constant can be derived which is generally expected to apply to low-lying vibrational levels. In electron-beam-pumped lasers, the two-body rate constant for relaxation by Ar has been found to lie between 2.5–$5\times10^{-11}\,\mathrm{cm^3\,s^{-1}}$ [6–8]. A similar rate constant has been found for Kr-buffered lasers [9]. Kannari et al. [8] have pointed out that such rates apply equally to the B and C states which are collisionally mixed under normal laser conditions and they derive a rate constant for $B-C$ transfer of $5\times10^{-10}\,\mathrm{cm^3\,s^{-1}}$ for an Ar buffer. In discharge lasers employing He buffers, Pummer et al. [10] measured lifetimes which implied a vibrational relaxation rate of $5\times10^{-12}\,\mathrm{cm^3\,s^{-1}}$ and a $B-C$ mixing rate $>2\times10^{-11}\,\mathrm{cm^3\,s^{-1}}$. In a similar system Szatmari and Schaefer [11] measured the gain recovery following saturation by a pulse of 10 ps duration. They attribute the lack of a two-component recovery time to a $B-C$ mixing time of <10 ps which would imply a rate constant of $>2\times10^{-9}\,\mathrm{cm^3\,s^{-1}}$ if two-body collisions

with helium were responsible! However, as Kannari et al. [8] point out, a single-component gain recovery curve would also be observed if the mixing rate was very much slower, i.e. comparable to the vibrational relaxation rate. On the other hand, it is possible that $B-C$ mixing under laser conditions is dominated by electron collisions, although the rate constant would need to be very large ($\simeq 10^{-5}$ cm^3 s^{-1}) to account for mixing on a picosecond timescale.

Obviously, the collision dynamics in the lasers themselves are highly complex and experiments need to be made under much simpler and more controlled conditions so that the various rate processes can be isolated as much as possible and measurements made with some degree of assurance as to what one is measuring. Fortunately, such measurements have previously been made on XeCl. Dreiling and Setser [12] used both flowing afterglow and resonance radiation techniques to produce XeCl* by reaction of chlorine donors with Xe*($^3P_2$ and $^3P_1$). By careful measurement of the $B\rightarrow X$ and $C\rightarrow A$ emission spectra as a function of buffer gas pressure, both vibrational relaxation and $B-C$ mixing rate constants were obtained for collisions with the rare gases. The general conclusions from this important work were:

a) Both rates increase in the order He < Ne < Ar.

b) Both rates depend on vibrational level and increase as v' increases.

c) Both rates are of comparable magnitude (except for the heavy gases at low v' where mixing dominates) and the sum of the rates is nearly gas kinetic at high v'.

Recently [13], laser photoassociation from Xe + Cl atoms has been used to produce even cleaner initial conditions whereby XeCl(B) is formed in known low-lying vibrational levels. Mixing and relaxation rates were obtained in a Xe buffer and tended to confirm the earlier work.

Because of its importance as a laser and the discrepancies between previous studies of mixing and vibrational relaxation in KrF (particularly as between e-beam-pumped and discharge-pumped lasers), we consider that an effort to improve our understanding of these processes in KrF is long overdue. Consequently, we have employed experimental techniques similar to those described in [12] to obtain KrF $B\rightarrow X$ spectra in various rare gas buffers. An inversion technique [14] is used to obtain vibrational distributions at different pressures which allows the evaluation of vibrational relaxation rates [15]. Using this method we have been able to obtain "effective" (see below) vibrational relaxation rates for KrF* in collisions with He, Ne, and Ar. We have also measured effective vibrational relaxation rate coefficients for XeCl* in collisions with Ar to compare with previous results.

Experimental

The KrF spectra were obtained at the University of Nottingham using a resonance radiation technique described in detail elsewhere [16]. Briefly, resonance radiation from Kr atoms ($\lambda = 123.6$ nm) excited by a microwave discharge passes through a LiF window into a fluorescence cell containing a mixture of Kr and NF_3 (0.25 + 0.25 Torr) plus a rare gas buffer. Some of the Kr atoms in the cell are excited to the resonance level Kr*($^3P_1$) and react to produce KrF* via

$$Kr^*(^3P_1) + NF_3 \rightarrow KrF^*(B, v' \leqq 53) + NF_2 . \quad (1)$$

Other excited states of KrF (i.e. C and D) are also produced in the initial reaction. The resulting fluorescence in the KrF $B\rightarrow X$ band is recorded as a function of pressure of various rare gases using a scanning monochromator (Hilger 0.6 m), photon counter and microcomputer for data acquisition. The raw data were transferred to a PDP 11/23 computer where they were corrected for spectral response, normalised and averaged at 200 cm^{-1} intervals for spectral inversion and comparison of experimental and recalculated spectra.

The same apparatus was used to excite XeCl spectra by reacting Xe*($^3P_1$) with Cl_2 which excites the B state up to $v' = 119$. XeCl spectra were also obtained in a flowing afterglow apparatus (at the University of Iceland) [15] and in this case Xe metastables ($^3P_2$) were reacted with Cl_2 and CCl_4 to produce XeCl (B) in vibrational levels up to $v' = 111$ and $v' = 65$, respectively. Buffer gas pressure in the resonance fluorescence apparatus could be varied over the range 0–760 Torr. In the flowing afterglow, the pressure range was limited to 0.5–6.0 Torr (the lower limit being set by wall losses and the upper by collisional deactivation of the metastables). In both cases the rare gases used were BOC research grade and were admitted to the systems through cryogenically-cooled, molecular-sieve traps. Pressures below 10 Torr were measured with a Baratron gauge or silicon oil manometer and above with a mercury manometer.

Results and Analysis

The KrF emission spectra were recorded over the spectral region 200–260 nm. It had been hoped to extend the spectral range to longer wavelengths to include the $C\rightarrow A$ emission between 300 and 400 nm [17]. However, in this region the rather weak KrF spectrum was overlaid by strong OH emission bands originating from water impurity which proved difficult to reduce to a level where quantitative measurements could be made.

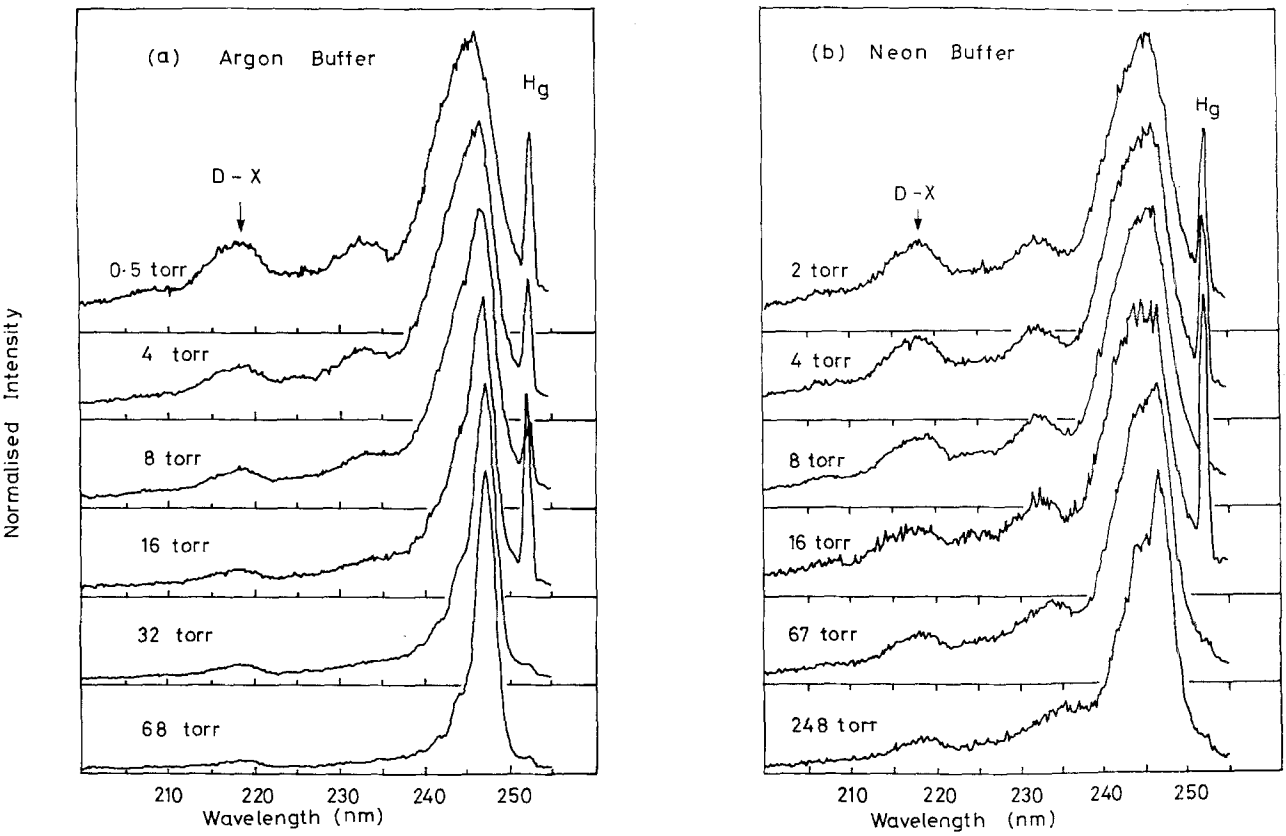

Fig. 1a, b. KrF $B \rightarrow X$ emission spectra excited by Kr resonance radiation illumination of 0.25 Torr Kr + 0.25 Torr NF_3 + buffer gas to total pressure shown. (a) Ar buffer; (b) Ne buffer

A typical set of spectra showing the changes in the $B \rightarrow X$ band profile as a function of both Ar and Ne buffer gas pressures is shown in Fig. 1a and b, respectively. The shape of the $D \rightarrow X$ band at 220 nm was found to be relatively insensitive to pressure compared with the $B \rightarrow X$ band indicating most probably that this band is formed in low-lying vibrational levels. The line feature at 254 nm is the Hg resonance line from Hg contamination in the lamp and/or reaction cell. It varied in intensity from run to run but did not appear to affect the KrF spectra in any way other than providing a convenient calibration wavelength. With Ar as buffer gas, almost complete relaxation was obtained at 68 Torr pressure. In contrast, with Ne as buffer, the spectra are still significantly unrelaxed at 248 Torr pressure. The He spectra behaved similarly to the Ne ones.

For comparison, Fig. 2 shows XeCl $B \rightarrow X$ spectra obtained from the flowing afterglow using Cl_2 as chlorine donor. Even over the limited pressure range available in this apparatus, significant vibrational relaxation can be seen to be taking place as the Ar pressure is increased from 0.6 to 4.8 Torr.

For both KrF and XeCl the steady-state vibrational population distributions in the $B(1/2)$ states were obtained by direct inversion of the $B \rightarrow X$ spectra

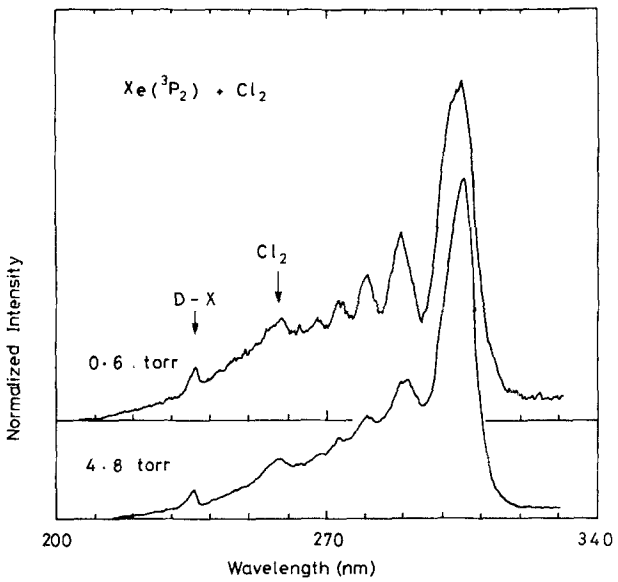

Fig. 2. XeCl $B \rightarrow X$ emission spectra from the reaction of Xe($^3P_2$) metastables with Cl_2 in a flowing afterglow with Ar buffer at 0.6 and 4.8 Torr

[14]. In order for this technique to be computationally tractable, the vibrational population is approximated by a histogram comprising n blocks (typically 4–10) each of which contains m vibrational levels (typically in

Table 1. Molecular parameters (r in Å)

KrF	XeCl
a) Potential for bound upper state (B state)	
$U'(r)=1.6748\times10^7\exp(-r/0.343289)$ $-1.1614\times10^5/r$ $-3.216\times10^5/r^4$ $+84065\ \mathrm{cm}^{-1}$	$U'(r)=2.6606\times10^7\exp(-r/0.4064)$ $-1.1249\times10^5/r$ $-10.914\times10^5/r^4$ $+67841\ \mathrm{cm}^{-1}$
$r_e=2.5335$ Å	$r_e=3.227$ Å
b) Potential for repulsive lower state (X state)	
$U''(r)=3123500/r^9\ \mathrm{cm}^{-1}$	$U''(r)=6.7972\times10^7\exp(-r/0.257)$ $-1.165\times10^5/r^6\ \mathrm{cm}^{-1}$
c) B state vibrational frequencies	
$G(v')=329.8549(v'+1/2)$ $-1.52583(v'+1/2)^2$ $+0.003420275(v'+1/2)^3\ \mathrm{cm}^{-1}$	$G(v')=194.235(v'+1/2)$ $-0.63152(v'+1/2)^2$ $+0.0009621(v'+1/2)^3\ \mathrm{cm}^{-1}$
d) $B\rightarrow X$ transition moment as a function of internuclear separation	
$\mu(r)=1.163/((r-2.35)^2+0.416)$	$\mu(r)=(20.88-21.229r+8.1968r^2$ $-1.4316r^3+0.09742r^4)^{-1}$ $\times\exp[0.4(r-4.9783)]$
e) Einstein A coefficient as a function of vibrational level	
$A(v')=1.400\times10^8-2.428\times10^6v'$ $+1.623\times10^4v'^2\ \mathrm{s}^{-1}$	$A(v')=9.0999\times10^7-6.7198\times10^5v'$ $-1.519\times10v'^2+24.192v'^3\ \mathrm{s}^{-1}$

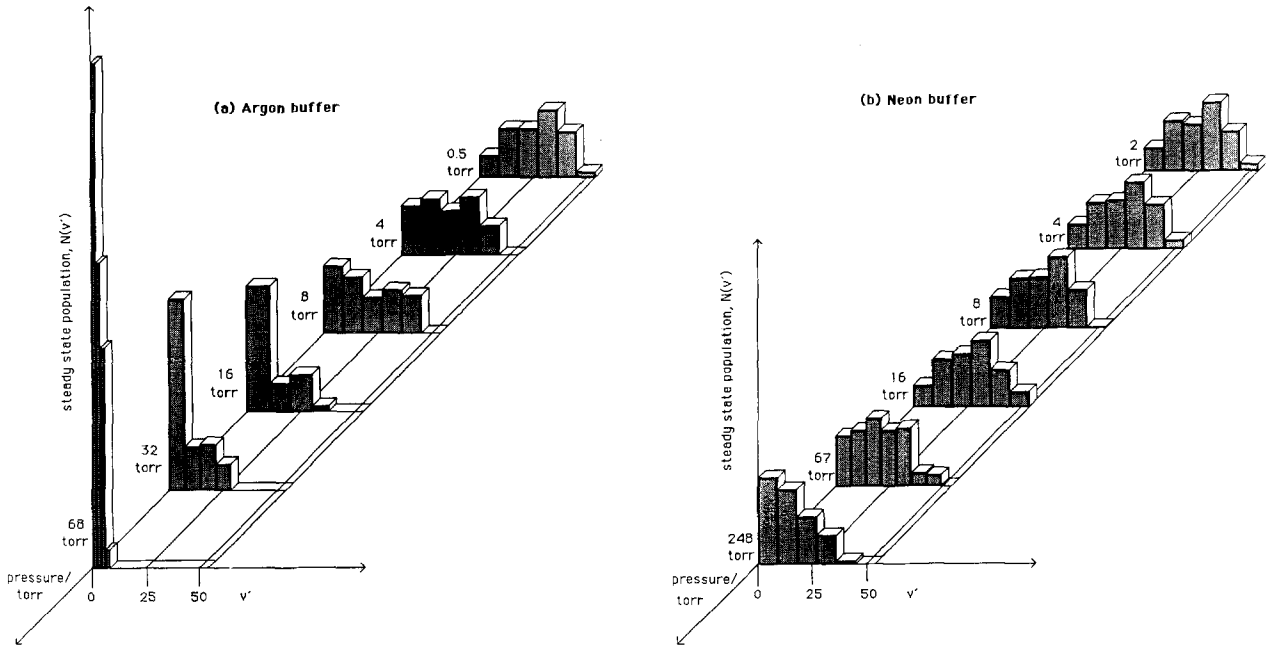

Fig. 3. Histograms of vibrational populations in the KrF B state corresponding to the spectra of Fig. 1. Histograms are normalised so that the total number of particles in each histogram is constant

the range 9–20). With a prior knowledge of the bound and free molecular potentials $U'(r)$ and $U''(r)$ as well as the transition moment $\mu(r)$, the population histogram can be generated from the observed spectra using multiple linear regression. The potential parameters used are listed in Table 1. They are based on the "ab initio" calculations of Hay and Dunning [18] as modified by small corrections introduced by Setser [17, 19] or by ourselves in order to optimise agreement between the observed spectral profiles and those calculated from the inversion and simulation procedures. In KrF only that part of the spectrum above the $D\rightarrow X$ band at 220 nm was fitted. The Cl_2 band in XeCl was similarly avoided. Figure 3 shows the steady-state vibrational populations for KrF (B) corresponding to the spectra in Fig. 1. The rapid vibrational relaxation

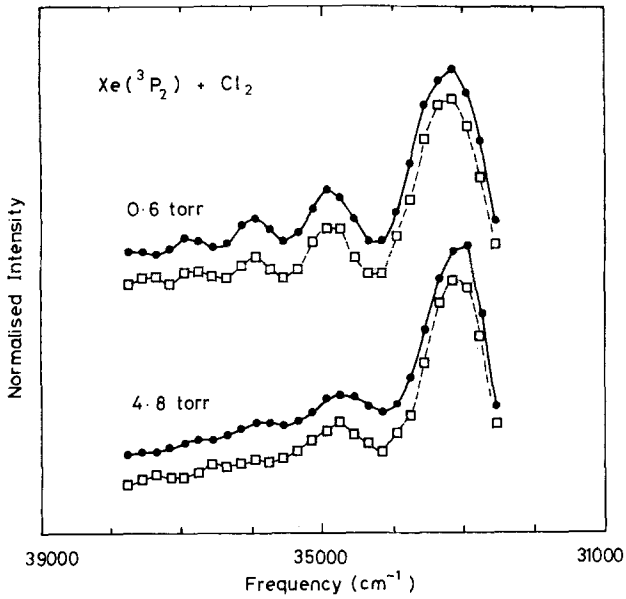

Fig. 4. XeCl $B \rightarrow X$ spectra. Solid line: as digitised from the experimental spectra shown in Fig. 2. Dotted line: spectra recalculated from the population histograms

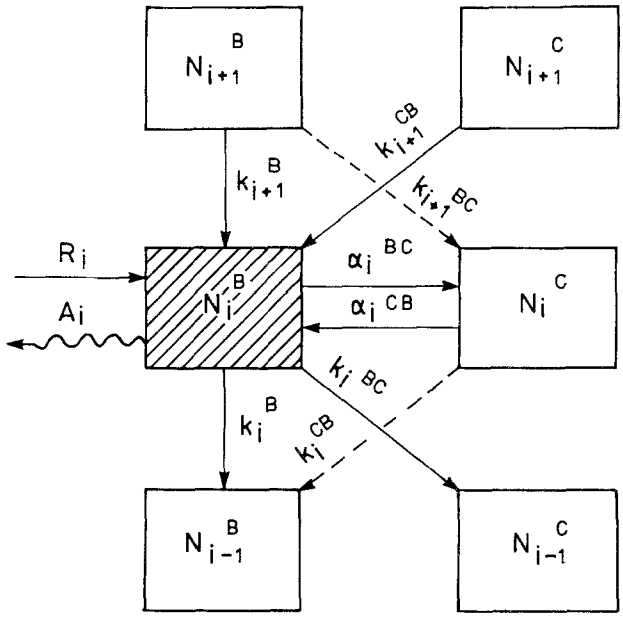

Fig. 5. Gain and loss processes affecting a single block of vibrational levels in the B state

in the case where Ar is the collision partner is clearly displayed, as is the contrast between Ar and Ne. Spectra calculated by re-inverting the population histograms were found to agree extremely well with the original digitised spectra. As an example Fig. 4 shows digitised and recalculated spectra for XeCl ($B \rightarrow X$) from the original data of Fig. 2.

Vibrational Relaxation Rates

With a knowledge of the vibrational population histograms of the B state, it is possible to define a vibrational relaxation rate constant k_i^B by

$$\mathrm{KrF}^*(B,i)+\mathrm{M} \xrightarrow{k_i^B} \mathrm{KrF}^*(B,i-1)+\mathrm{M} \qquad (2)$$

which results in the transference of a molecule from one block to the next lowest in the population histogram. Unfortunately, these intra-state relaxation rates are not directly observable due to inter-state processes between the B and C states which also contribute to vibrational relaxation. We can, however, use our data to evaluate an "effective" relaxation rate constant which is the sum of the intra and inter-state relaxation rate constants as we show below.

With reference to Fig. 5 we can write the steady-state rate equation for the population N_i^B in the ith block of levels of the B state by

$$\frac{dN_i^B}{dt} = R_i - A_i N_i^B + k_{i+1}^B N_{i+1}^B[\mathrm{M}] + k_{i+1}^{CB} N_{i+1}^C[\mathrm{M}] + \alpha_i^{CB} N_i^C[\mathrm{M}] - k_i^B N_i^B[\mathrm{M}] - k_i^{BC} N_i^B[\mathrm{M}] - \alpha_i^{BC} N_i^B[\mathrm{M}] = 0, \qquad (3)$$

where A_i is the Einstein coefficient for the vibrational level at the midpoint of the block, and R_i is the pump rate into the block due to the formation reaction. Since we have no measurements of the C state populations we cannot solve these equations directly and simplifying assumptions have to be made. These are difficult to make in the low pressure region where collisional and radiative rates are comparable. There is, however, a broad pressure range over which collisions are expected to maintain a dynamic equilibrium leading to a constant $B:C$ population ratio. By measuring this ratio from the fluorescence on the $B \rightarrow X$ relative to the $C \rightarrow A$ bands, Setser et al. [12, 20, 21] found for the xenon halides that the ratio initially increases with Ar pressure but then remains constant over a pressure range from a few to a few hundred Torr. At still higher pressures the ratio falls as the low-lying vibrational levels of the C state which lie below the B state become populated. In the intermediate pressure range we can thus assume that on a block-by-block basis the transfer rate from B to C is matched by the transfer rate from C to B, i.e.

$$\alpha_i^{BC} N_i^B = \alpha_i^{CB} N_i^C, \qquad (4)$$

$$k_i^{BC} N_i^B = k_i^{CB} N_i^C, \qquad (5)$$

for all i. These expressions may be used to eliminate the C state populations from (3) giving a rate equation involving the B state alone which (on dropping the superscripts) becomes

$$\frac{dN_i}{dt} = R_i - A_i N_i + k'_{i+1} N_{i+1}[\mathrm{M}] - k'_i N_i[\mathrm{M}] = 0, \qquad (6)$$

Table 2. Vibrational energy disposal

Reaction	$Kr(^3P_1)+NF_3$	$Xe(^3P_1)+Cl_2$	$Xe(^3P_2)+Cl_2$	$Xe(^3P_2)+CCl_4$
Vibrational levels/block	9	20	16	11
v'_{max} [a]	53	119	111	65
Population rates R_i [b]				
$i=1$	0.143	0.036	0.043	0.021
$i=2$	0.245	0.053	0.116	0.099
$i=3$	0.211	0.133	0.128	0.149
$i=4$	0.244	0.277	0.140	0.238
$i=5$	0.144	0.335	0.197	0.336
$i=6$	0.014	0.167	0.283	0.158
$i=7$			0.093	

[a] Maximum excited level in population histogram; $v'_{max}=(n\times m)-1$

[b] Rates normalised to $\sum_i R_i=1$

where the rate constants k'_i are given by

$$k'_i=k_i^B+k_i^{BC} \tag{7}$$

and thus represent effective rate constants which are the sum of the interstate and intra-state relaxation rate constants.

With this interpretation of the rate constants the set of equations (6) may be solved. The rates R_i may be determined from the steady-state population distribution in the low pressure limit, N_i^0 via the relation $R_i=A_iN_i^0$. These rates give information on the vibrational disposal of energy from the initial formation reaction and are given in Table 2. With these expressions for R_i we can obtain a recurrence relationship for the effective relaxation rate constants:

$$k'_{i+1}=[k'_iN_i[M]+A_i(N_i-N_i^0)]/N_{i+1}[M]. \tag{8}$$

The proceedure is started at the lowest block, $i=1$ since its relaxation rate is by definition zero giving

$$k_2=A_1(N_1-N_1^0)/N_2[M] \tag{9}$$

from which follow the rate constants for the higher levels. It should be noted that the rate constants are solely determined by the population histogram at a single pressure (compared with that at very low pressure) and thus it is possible to determine the rate constants as a function of pressure using this technique.

Implicit in this analysis there are two further assumptions which we need to discuss. Firstly, we have assumed that relaxation only occurs to the nearest neighbour block. The validity of this assumption will depend upon the number m of vibrational levels per block. If these are too few, the neglect of relaxation to non-nearest neighbour groups will be unjustified. If there are too many, then the resolution of the vibrational distribution will be poor and information will be lost. In practice, the true level-to-level rate constants for vibrational relaxation can be expected to follow an exponential energy-gap law [22]. Thus relaxation into levels lying beyond the nearest neighbour group will diminish rapidly as m increases. We seek, therefore, a compromise selection of the data resolution, which varies m/n to a limiting value above which constant and consistent values for the set of rate coefficients k_i are obtained. Secondly, (3) assumes that quenching is unimportant compared with radiative losses. In laser mixtures the dominant quenching process is trimer formation via three-body processes such as

$$KrF^* + Kr + M \rightarrow Kr_2F^* + M. \tag{10}$$

Since our experiment avoids resonant buffer gases (Kr for KrF, and Xe for XeCl), the quench rate due to (10) [23] is very much slower than the radiative losses even at the highest pressures used in our experiments. Estimates of two-body quench rates [8] also turn out to be two orders of magnitude slower than the vibrational rates which we derive.

The validity of the assumptions in this analysis can be tested by comparing the evaluations of rate constants made at different pressures in the pressure region where we expect $B:C$ equilibrium. When this was done generally good agreement was found, for example in KrF+Ar measured at 4, 8, and 16 Torr and for KrF+Ne measured at 67 and 248 Torr. Measurements made at 4.8, 5.4, and 10.2 Torr in XeCl+Ar are plotted in Fig. 6 and compared with the previous results obtained by Dreiling and Setser [12]. Again good agreement is found. Table 3 assembles the results for both KrF and XeCl. The rate constants from [12],

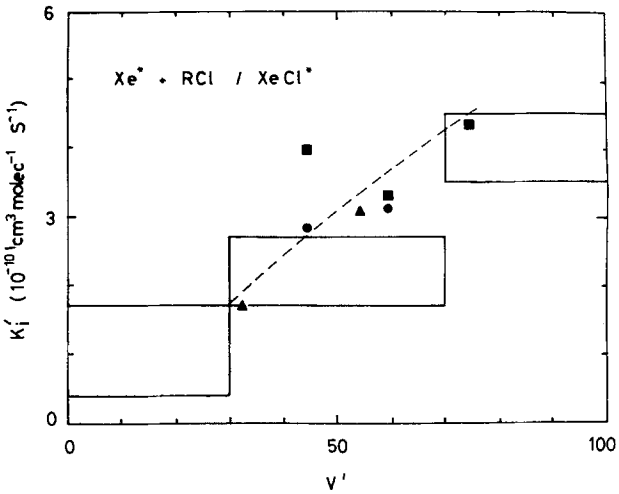

Fig. 6. Effective vibrational relaxation rate constants as a function of vibrational level for XeCl+Ar. Triangles: $Xe(^3P_2)+CCl_4$ at 4.8 Torr, circles: $Xe(^3P_1)+Cl_2$ at 10.8 Torr, squares: $Xe(^3P_1)+Cl_2$ at 5.4 Torr. The large open boxes give the limits of the sum of relaxation and inter-system crossing rate constants from [12]

Table 3. Vibrational relaxation rate constants

v'	M=He	M=Ne	M=Ar
KrF(B, v')+M(10^{-11} cm^3 s^{-1})			
13	0.8±0.5	1.2±0.5	42±12
19			42±23
22	2.5±0.5	2.5±0.8	58±12
31	3.0±0.7	3.5±0.8	42±17
40	4.0±1.2		
XeCl(B, v')+M(10^{-11} cm^3 s^{-1})[a]			
4–30	0.65–2.9	1.2–5.5	4–17 (17 ± 5 at $v'=33$)[b]
30–70	2.9 –5.0	5.5–9.7	17–27 (31 ± 9 at $v'=60$)[b]
70–130	5.0 –6.9	9.7–13.0	35–45 (43 ± 13 at $v'=75$)[b]

[a] Sum of intersystem and vibrational rate constants from [12]
[b] This work

included for comparison, are the sum of the relaxation and intersystem crossing rate constants which should be equivalent to our "effective" rate constant. The agreement is very good in the one overlapping case of XeCl+Ar. This adds confidence to our assertion that the rate constants which we derive may be directly compared to the sum rates from [12].

Discussion and Relevance to Laser Processes

As Table 3 shows, there is a remarkable similarity between the relaxation rate constants for KrF and XeCl, both in the trend with collision partner and vibrational level and in the absolute magnitude. The only exception is KrF+Ar where the rate constant is relatively invariant with vibrational level instead of increasing as in the XeCl+Ar case. It should, however, be noted that if the rate constant increased much above the measured value it would greatly exceed the gas-kinetic collision rate.

When these results are compared with measurements made under laser conditions there are some agreements and some discrepancies. Our KrF+Ar result is in exact agreement with the intersystem crossing rate constant of Kannari et al. [8], but their intra-system relaxation rate constant is an order of magnitude less. Since we only derive the sum rate we could not observe this effect. Furthermore we could not obtain rate constants for the very lowest levels and it may well be that the intra-state relaxation rate constant falls rather rapidly as v' tends to zero.

For the case of He buffers our results compare resonably well with the observations of Pummer et al. [10], however there is no indication of the very large rate constant which would be required to explain $B-C$ mixing by He collisions on a picosecond timescale, as suggested by Szatmari and Schaefer [11]. It also seems very unlikely that electron collisions can be invoked to explain such rapid mixing. If electrons were so to dominate the $B-C$ mixing rates, the $B:C$ population ratio of the low lying levels would be determined by the electron temperature which in both e-beam and discharge lasers will be considerably higher than the gas temperature. This ratio has been measured as a function of beam current in an e-beam excited XeCl laser [24] and recently at high current density in a discharge excited XeCl laser [25]. In both cases the $B:C$ ratio was found to be identical to the ratio measured at high pressure under electron free conditions [12, 20, 21]. Given the similarities between XeCl and KrF, it would be very surprising if this result could not also be applied to KrF.

The most likely explanation of the single exponential gain recovery observed in [12] is that the intersystem and vibrational lifetimes were of comparable magnitude to the quenched lifetime of the B state. This conclusion does not effect the picosecond gain dynamics of the laser however, since the C state in KrF will, on a picosecond timescale, simply act as a reservoir of excited state population in much the same way as the higher vibrational levels of the B state. Verification of this conclusion awaits the measurement of the C state population as the B state is depleted by a picosecond pulse. In this measurement the difference between picosecond and nanosecond mixing will be easily observable.

Acknowledgement. The authors are grateful for the helpful comments of F. Kannari, Spectra Technology Inc., USA

References

1. A.D. Schwarzenbach, T.S. Luk, I.A. McIntyre, U. Johann, A. McPerson, K. Boyer, C.K. Rhodes: Opt. Lett. **11**, 499 (1986)
2. J.H. Glownia, G. Arjavalingam, P.P. Sorokin, J.E. Rothenberg: Opt. Lett. **11**, 79 (1986)
3. W.L. Morgan, N.W. Winter, K.C. Kulander: J. Appl. Phys. **54**, 4275 (1983)
4. J.H. Jacob, J.C. Hsia, J.A. Mangano, M. Rokni: J. Appl. Phys. **50**, 5130 (1979)
5. L.A. Rosocha, P.S. Bowling, M.D. Burrows, M. Kang, J. Hanlon, J. McLeod, G.W. York, Jr.: Laser Part. Beams **4**, 55 (1986)
6. K.V. Gratton, M.H.R. Hutchinson, K.J. Thomas: Opt. Commun. **39**, 303 (1981)
7. J.H. Jacob, D.W. Trainor, M. Rokni, J.C. Hsia: Appl. Phys. Lett. **37**, 552 (1980)
8. F. Kannari, M. Obara, T. Fujioka: J. Appl. Phys. **57**, 4309 (1985)
9. F. Kannari, M.J. Shaw, F. O'Neill: J. Appl. Phys. **61**, 476 (1986)
10. H. Pummer, K. Hola, F. Rebentrost: Appl. Phys. **20**, 129 (1979)
11. S. Szatmari, F.P. Schaefer: Appl. Phys. B **33**, 219 (1984)
12. T.D. Dreiling, D.W. Setser: J. Chem. Phys. **75**, 4360 (1981)
13. G. Inoue, J.K. Ku, D.W. Setser: J. Chem. Phys. **80**, 6006 (1984)
14. K. Johnson, A. Kvaran, J.P. Simons: Molec. Phys. **50**, 981 (1983)
15. A. Kvaran, I.D. Sigurdardottir, J.P. Simons: J. Phys. Chem. **88**, 6383 (1984)
16. K. Johnson, J.P. Simons, P.A. Smith, C. Washington, A. Kvaran: Mol. Phys. **57**, 255 (1986)
17. K. Tamagake, D.W. Setser: J. Chem. Phys. **67**, 4370 (1977)
18. P.J. Hay, T.H. Dunning, Jr.: J. Chem. Phys. **66**, 1306 (1977), ibid **69**, 2209 (1978)
    T.H. Dunning, P.J. Hay: Appl. Phys. Lett. **28**, 649 (1976)
19. K. Tamagake, D.W. Setser, J.H. Kolts: J. Chem. Phys. **84**, 224 (1980)
20. Y.C. Yu, D.W. Setser, H. Horiguchi: J. Chem. Phys. **87**, 2199 (1983)
21. K. Tamagake, D.W. Setser, J.H. Kolts: J. Chem. Phys. **74**, 4286 (1981)
22. N.H. Cheung, T.A. Cool, A.C. Erlandson: J. Chem. Phys. **86**, 6203 (1987)
23. M. Rokni, J.H. Jacob, J.A. Mangano: Phys. Rev. A **16**, 2216 (1977)
    M. Rokni, J.A. Mangano, J.H. Jacob, J.C. Hsia: IEEE J. QE-**14**, 464 (1978)
24. T.G. Fin, R.S.F. Chang, L.J. Palumbo, L.F. Champagne: Appl. Phys. Letts. **36**, 789 (1980)
25. D. Lo, C.E. Zheng: J. Phys. D **20**, 717 (1987)